Research Square

Preprints are preliminary reports that have not undergone peer review.
They should not be considered conclusive, used to inform clinical practice,
or referenced by the media as validated information.

Development of Rainfall–R-factor Models and Trend Analysis of Rainfall Erosivity across Selected Agro-Ecological Sub-Regions of India

Ch. Jyotiprava Dash
ICAR-Indian Institute of Soil and Water Conservation
Shashi Sekhar Shrimali
Indian Institute of Soil and Water Conservation
Shakir Ali
Indian Institute of Soil and Water Conservation
Kamal Kishor Sharma
Indian Institute of Soil and Water Conservation
Uday Mandal
Indian Institute of Soil and Water Conservation
B. S. Naik
ICAR-Indian Institute of Soil and Water Conservation
H. C. Hombegowda
ICAR-Indian Institute of Soil and Water Conservation
M. Madhu
ICAR-Indian Institute of Soil and Water Conservation
Pravat Ranjan Ojasvi
Indian Institute of Soil and Water Conservation
Prashant Kumar Mishra
Indian Institute of Soil and Water Conservation
Partha Pratim Adhikary
partha.adhikary@icar.org.in

ICAR-Indian Institute of Soil and Water Conservation

Research Article

Keywords: Soil erosion, I30-based R-factor, Erosivity density, Innovative Trend Analysis, Conservation measure

Posted Date: November 25th, 2026

DOI: https://doi.org/10.21203/rs.3.rs-11676174/v1

License: This work is licensed under a Creative Commons Attribution 4.0 International License.
Read Full License

Additional Declarations: No competing interests reported.

Development of Rainfall–R-factor Models and Trend Analysis of Rainfall Erosivity across Selected Agro-Ecological Sub-Regions of India

Abstract

Reduced agricultural yields and nutrient depletion are consequences of soil erosion, which is worsened by climate change. This calls for precise soil erosion measurement, in an agrarian country like India. The rainfall erosivity factor (R-factor) is an important component of the widely used universal soil loss equation (USLE) for quantifying potential soil. In comparision to the Modified Fournier Index (MFI) or hourly and daily rainfall data, the R-factor calculated based I_{30} derived from sub-hourly rainfall data is more accurate. However, still, most locations do not have sub-hourly rainfall information available. Therefore, in this study, rainfall-R-factor models were developed for eight Agro-Ecological Sub Regions (AESRs) of India (3.0, 4.1, 4.4, 5.2, 9.1, 12.1, 14.2 and 19.2). Further, for analyzing temporal trends in erosive rainfall and R-factor, Innovative Trend Analysis (ITA) and Mann-Kendall (MK) were used. While the other AESRs showed a power relationship, AESRs 4.4 and 9.1 showed a linear relationship between annual rainfall and annual R-factor. Six AESRs (3.0, 4.1, 4.4, 5.2, 12.1 and 14.2) exhibited increasing trends for both erosive rainfall and R-factor, while AESRs 9.1 and 19.2 exhibited decreasing trends. R-factors calculated from IMDAA hourly rainfall data were generally lower than the I_{30} based R-factor, except for the low rainfall regions. The monthly erosivity density during monsoon exceeded the critical threshold in all AESRs indicating a substantial risk of water-induced soil erosion. The findings confirm the necessity for localised rainfall-R-factor models and soil and water conservation strategies.

Key words: Soil erosion, I_{30}-based R-factor, Erosivity density, Innovative Trend Analysis, Conservation measure

Highlights

1. AESR-4.4 and AESR-9.1 showed linear relationships between the R-factor and annual rainfall, whereas AESRs 3.0, 4.1, 5.2, 12.1, 14.2 and 19.2 showed power relationships.

2. The mean annual I_{30} based R-factor ranged from 2,451.83 MJ mm ha^{-1} hr^{-1} yr^{-1} in AESR-3.0 to 10,014.64 MJ mm ha^{-1} hr^{-1} yr^{-1} in AESR-14.2.

3. Increasing trends in erosive rainfall and R-factor were observed in AESRs 3.0, 4.1, 4.4, 5.2, 12.1 and 14.2, whereas AESRs 9.1 and 19.2 exhibited decreasing trends.

4. R-factor estimates derived from IMDAA hourly and IMERG sub-hourly rainfall datasets underestimated annual rainfall erosivity across all selected AESRs compared with I_{30}-based estimates.

1. Introduction

Soil erosion is one of the major types of land degradation, which is detrimental to ecosystem health and sustainable land management, because it slowly removes the top fertile soil, exposes the subsurface and causes sedimentation in the aquatic system, which leads to contamination of aquatic ecosystems and reduces the capacity of water bodies. Further, this process reduces soil's water holding capacity led by depletion of soil organic matter (SOM), which in turn adversely affects agricultural productivity and growth of natural vegetation (Lee & Heo, 2011; Adhikary et al., 2018). This primarily calls for soil loss quantification-based implementation of suitable location specific soil conservation measures and sustainable land-use planning.

Quantification of soil loss is widely done using Universal Soil Loss Equation (USLE), in which potential soil erosion is calculated by multiplying six factors i.e. soil erodibility, slope length and gradient, vegetation cover, supporting conversion practices, and rainfall erosivity factor (R-factor). Among these factors, the R-factor is very important because it reflects the kinetic energy (KE) of rainfall, which is the main driver of soil erosion. The R-factor is expressed as the product of the KE of rainfall and the maximum 30-minute rainfall intensity (I_{30}), also known as EI_{30}. As the sub-hourly rainfall data is not available everywhere, researchers generally correlate the R-factor with daily, monthly, and annual rainfall data (Liu et al., 2013; Hernando & Romana, 2015; Yang & Yu, 2015; Dash et al., 2019; Das et al., 2022; Fenta et al., 2024). While monthly and daily rainfall are only available in certain locations, annual rainfall is widely available for all regions.

The first annual R-factor map on a national scale for India was developed by Rambabu et al. (1978), while recently during 2015, a R-factor map of India was developed using Modified Fournier Index (MFI), based on monthly rainfall (Tiwari et al., 2016). Similarly, Raj et al. (2022) developed an R-factor map of India based on three gridded datasets, namely, hourly Indian Monsoon Data Assimilation and Analysis, daily India Meteorological Department (IMD) and daily CHIRPS with temporal resolutions of 1 hour, 1 day and 1 day, respectively. The first method estimated the R-factor by using the I_{60} values. The latter two datasets were employed for estimating the Fournier Index (FI) and MFI. Further, a study carried out on the spatial pattern and monthly distribution of R-factor over India based on IMD hourly rainfall data (1969 to 2021) using 261 rain gauge stations by I_{60} approach (Das et al., 2025). Results from the Eastern Ghats of India and central Chile, showed that R-factor values derived from I_{60} tend to be underestimated (Dash et al., 2018; Lobo & Bonilla, 2015). The underestimation of the R-factor was also reported by Yin et al. (2007), Panagos et al. (2015), and Tu et al. (2023) when the time steps were extended from 5, 10, 15, 30, to 60 minutes. For Taiwan, the ratio of R-factor to mean R-factor calculated using I_{30} and I_{60} methods were 1.30 and 1.47 respectively (Lee & Hsu, 2021). A recent study reported underestimation of R-factor by 4.5%, 8.0%, 9.6% and 5.8% respectively in comparison with R-factor estimates based on one-minute rainfall intensity in the arid climate of India (Machiwal et al., 2025). They also reported a 96.7% underestimation of the R-factor computed from daily rainfall. Further, a R-factor map was developed from high-resolution Integrated Multi-satellitE Retrievals for GPM (IMERG) final run 30-minute data (2001 to 2018) for India (mean annual R-factor ranged from 77 to 20,662 MJ mm ha^{-1} hr^{-1} yr^{-1}, and correlated R-factor to the daily rainfall using power equation (Das et al., 2022). The performance of CHRIPS, IMERG, and Precipitation Estimation from Remotely Sensed Information using Artificial Neural Networks (PERSIANN) Climate data record were compared for quantifying R-factor in the topographically and climatically

diverse Tensift watershed, west-central region of the Moroccan kingdom and highlighted the need for regional validation before selecting a satellite precipitation product for R-factor assessment (Daoud et al., 2024). Even though IMERG data are available in 30-minute time steps, it might be unable to accurately represent peak short-duration intensities associated to sub-30-minute rainfall variability, which tends to smooth high-intensity and extreme rainfall data, leading to underestimation of erosive events (Thakur et al., 2020; Das et al., 2022; Das et al., 2025). The gridded data have their own shortcomings in the way they are obtained and derived. In addition, local convective rainfall is averaged by spatial interpolation and coarse grid resolution, which reduces spatial variability and masks extreme occurrences, particularly in diverse or hilly terrain (Bezak et al., 2022; Fenta et al., 2023; Das et al., 2025).

Not only the rainfall-R-factor models are important, the long-term trends of erosive rainfall and R-factor are also significant for assessing the impact of climate change on soil erosion. The Intergovernmental Panel on Climate Change (IPCC) reported that frequency and intensity of heavy precipitation events have increased over many regions and are projected to increase further due to global warming (IPCC, 2023). It was reported that the frequency and intensity of extreme rainfall events in India increased significantly over central India despite no significant trend in seasonal mean rainfall (Goswami et al., 2006). Since R-factor is mainly controlled by rainfall intensity and kinetic energy, such changes are likely to affect the risk of soil erosion. However, long-term studies on I_{30} based rainfall erosivity in India are scarce because of the limited availability of sub-hourly rainfall records (Dash et al., 2024a). Hence, the study of long-term trends of erosive rainfall and R-factor is important for improving soil erosion assessment and developing region-specific soil and water conservation strategies.

In a vast, heterogeneous, agrarian country like India, where the agricultural productivity is influenced by climate, soil, topography, and other ecological factors, homogeneous zoning is important to manage the agricultural system properly. Homogeneous areas in India have been delineated and characterized by a number of agencies based on soil, climate, physiography and other related factors (Murthy & Pandey, 1978; Planning Commission of India, 1990). ICAR-National Bureau of Soil Survey and Land Use Planning has divided the entire India into 20 Agro-Ecological Regions (AERs) on the basis of length of growing period as an integrated criterion of effective rainfall and soil groups (Sehgal et al., 1992). Further these 20 AERs were divided into 60 Agro-Ecological Sub-Regions (AESRs) (Sehgal et al., 1996). Such regionalisation provides a proper framework for the development of location-specific R-factor models and soil conservation strategies.

Although several studies have estimated the R-factor for India using rainfall indices or gridded rainfall products, region-specific rainfall-R-factor relationships based on gauged sub-hourly rainfall data are still lacking. To address this gap, the present study develops rainfall-R-factor models for eight representative AESRs of India using I_{30}-based R-factor computed from sub-hourly rainfall observations. The study also analyses long-term trends in erosive rainfall and R-factor using the Mann-Kendall (MK) test and Innovative Trend Analysis (ITA). Furthermore, the developed models are used to estimate and map the spatial distribution of annual R-factor and erosivity density (ED) for the selected AESRs. The results provide a scientific basis for improving soil erosion assessment and for planning region-specific soil and water conservation measures under changing climatic conditions.

2 Materials and methods

2.1 Study area

The study area covers 8 AESRs of India, namely AESR 3.0, 4.1, 4.4, 5.2, 9.1, 12.1, 14.2, and 19.2, occupies almost 75 M ha of area and accounts for roughly 23% of the total geographical area of the country (Fig. 1). It includes states such as Andhra Pradesh (AP), Bihar, Chhattisgarh, Delhi, Goa, Gujarat (GJ), Haryana, Himachal Pradesh (HP), Jharkhand (JH), Karnataka (KN), Kerala, Madhya Pradesh (MP), Maharashtra (MH), Odisha, Punjab, Rajasthan (RJ), Tamil Nadu (TN), Telengana, Uttar Pradesh (UP), Uttarakhand (UK) and West Bengal (WB), along with three Union Territories (UT) namely Chandigarh, Daman & Diu and Jammu & Kashmir (J&K) (Table 1). The selected AESRs collectively represent all the major climatic ecosystems in the country. The ecosystems in the study area vary from arid conditions in AESR-3.0 to semi-arid conditions in AESRs 4.1, 4.4 and 5.2. On the other hand, AESRs 9.1, 12.1 and 14.2 are under sub-humid regions. AESR-19.2 is a coastal humid ecosystem. The characteristics of each AESR are presented in Table 1.

AESR-3.0 is a low-rainfall region (300-500 mm annual rainfall) and AESRs 9.1, 12.1, 14.2 and 19.2 are high-rainfall regions. Soils differ across the AESRs with mixed red and black soils in AESRs 3.0 and 4.4, deep black soils in AESR-5.2, deep alluvial soils in AESRs 4.1 and 9.1, red and lateritic soils in AESRs 12.1 and 19.2 and brown forest and podzolic soils in AESR-14.2. AESR-3.0 had the highest average annual temperature and shortest growing period (60-90 days), and the lowest temperature was in AESR-14.2 and the longest growing period (210-240 days) was in AESR-19.2. The AESRs have different climates and physiography, resulting in different agricultural practices. The agriculture in AESRs 3.0, 4.4, 12.1 and 14.2 is mainly rain-fed and the crops cultivated are sorghum, millets, pulses, maize, wheat and horticultural crops. However, AESRs 4.1 and 9.1 are related to intensive irrigated rice-wheat systems while AESR-5.2 is characterised by double cropping systems like soybean-wheat, groundnut and cotton. AESR-19.2 supports intensive rice cultivation interspersed with plantation crops such as coconut, cashew, arecanut, rubber, coffee and cocoa. Soil erosion also varies across the AESRs. Wind erosion, gully erosion and surface sealing affect the arid and semi-arid regions (AESRs 3.0, 4.1, 4.4 and 5.2) (Naik et al., 2021; Singh et al., 2023), but severe water erosion, including rill and gully formation, mass erosion and nutrient leaching, are observed in the sub-humid and humid regions (AESRs 9.1, 12.1, 14.2 and 19.2) (Dash et al., 2023; Hombegowda et al., 2021; Kannan et al., 2021; Panwar et al., 2023).

2.2 Data acquisition and development of rainfall and R-factor relation

For the development of R-factor model and subsequent mapping and trend analysis at various AESRs of India, the following datasets were used.

a) The sub-hourly rainfall data of eight meteorological observatory of ICAR-Indian Institute of Soil and Water Conservation (IISWC), Dehradun, India such as Research Centre (RC) Bellary, Karnataka (AESR-3.0), Agra, Uttar Pradesh (AESR-4.1), Datia, Madhya Pradesh (AESR-4.4), Kota, Rajasthan (AESR-5.2), Chandigarh, Punjab (AESR-9.1), Koraput, Odisha (AESR-12.1), Head Quarter, Dehradun, Uttarakhand (AESR-14.2),Udhagamandalam, Tamil Nadu (AESR-19.2).

b) Daily IMD gridded rainfall data with spatial resolution of 0.25 degree.

The sub-hourly rainfall data were used for computation of KE and subsequently the R-factor. The details of data period for each self-recording rain gauge are presented in Table 2. According to various studies (Wischmeier & Smith, 1978; Panagos et al., 2016; Dash et al., 2018), the threshold for erosive rainfall was 12.7 mm, with a 6-hour gap between rainstorms. Based on the slope of the hyetograph, the duration of each erosive event was divided into multiple time intervals. The rainfall intensity of each interval was then estimated (Dash et al., 2019). Afterward, the kinetic energy (KE_i) in MJ mm/ha for every interval was calculated using the equation given by Brown and Foster (1987).

$$KE_i = 0.29[1 - 0.72\exp(-0.05 i_r)] \dots (1)$$

where, i_r is the rainfall intensity for each interval (mm h^{-1}).

The R-factor for a single event (R_e, MJ mm ha^{-1} h^{-1}) was determined by multiplying KE with I_{30}. Taking the sum of the daily R-factor readings, the annual R-factor (R_a) (MJ mm ha^{-1} hr^{-1} yr^{-1}) was calculated.

The correlations between annual rainfall and the annual R-factor for all eight AESRs were established utilizing linear ($R = a \times P + b$), power ($R = a \times P^b$), logarithmic ($R = a \times \ln(P) + b$), exponential ($R = a \times e^{bP}$), and polynomial ($R = a \times P^2 + b \times P + c$) regression models, with P representing annual rainfall and a, b, and c denoting constants. The most suitable regression model from the aforementioned options was selected according to the highest coefficient of determination (R^2) (Dash et al., 2019). Seventy five percent of data was used for model development (model calibration) and 25% for model validation. Further, the performance of model was evaluated using Nash-Sutcliffe model efficiency (NSE) (Nash & Sutcliffe, 1970), Root Mean Square Error (RMSE), and Percent Bias (PBIAS) values (Moriasi et al., 2007). The performance of the model regarded as very good, good, satisfactory and unsatisfactory when the NSE values observed to be above 0.75, between 0.65 and 0.75, between 0.50 and 0.65 and less than or equal to 0.50, respectively. Similarly, PBIAS values within ±10% are classified as very good, ±10% to ±15% as good, ±15% to ±25% as satisfactory, and values exceeding ±25% as unsatisfactory. Positive PBIAS values indicate model underestimation, whereas negative values reflect overestimation (Moriasi et al., 2007). Given that only one sub-hourly rainfall data was available for each AESR, the daily IMD gridded rainfall dataset was used to estimate the R-factor at each IMD gridded points using the developed AESR-specific empirical models. This allowed for a comprehensive evaluation of the spatial variability of the R-factor and the corresponding ED across all AESR.

2.3 Erosivity density

The substantial temporal and spatial variability in rainfall and R-factor values, along with requirement of lengthy rainfall records (> 20 years) for robust long-term R-factor estimation, leads to development of erosivity density concept (Foster et al., 2008). It provides a more stable and data efficient alternative by expressing the erosive power of rainfall per unit rainfall (Eq.2). Numerous studies have shown that ED is less sensitive to missing data, requires shorter rainfall records, and remains relatively independent of elevation up to approximately 3000 m. Consequently, it is widely used to characterize spatial patterns of R-factor, particularly in regions with limited or uneven rainfall intensity measurements (Foster et al., 2008; Dabney et al., 2011; Panagos et al., 2015; Dash et al., 2019; Das et al., 2025).

185 $$Erosivitydensity\,(MJ/ha/hr) = \frac{R-factor}{P} \ldots (2)$$

186

187 **2.4 Erosive rainfall and R-factor trend analysis**

188 In the present study, the Mann-Kendall (MK) test was used to see the trend in erosive rainfall (Mann, 1945) and R-
189 factor, as its usefulness was reported by many researchers in determining the linear trend of annual rainfall, MFI,
190 erosive rainfall and R-factor (Dash et al., 2020; Gu et al., 2020; Dash et al., 2024a; Gu et al., 2025). The present study
191 assumes null hypothesis (H_0) as no trend whereas, the alternate hypothesis (H_1) assumed the presence of a trend in the
192 data. The expression of trend is as follows:

193 $$S = \sum_{j=1}^{m-1} \sum_{k=j+1}^{m} sign\left(x_k - x_j\right) \ldots (3)$$

194 $$Sign(x_k - x_j) = \begin{cases} 1 & if \quad x_k > x_j \\ 0 & if \quad x_k = x_j \\ -1 & if \quad x_k < x_j \end{cases} \ldots (4)$$

195 $$Mean(S) = 0, \qquad Variance(S) = \frac{m(m-1)(2m+5)}{18} \ldots (5)$$

196 $$Z = \begin{cases} \dfrac{S-1}{\sqrt{Variance(S)}} & if \quad S > 0 \\ 0 & if \quad S = 0 \\ \dfrac{S+1}{\sqrt{Variance(S)}} & if \quad S < 0 \end{cases} \ldots (6)$$

197 where x_j and x_k are the climatic variables at time j and k respectively, m is the length of data period, sign is the sign
198 function. The increasing and decreasing trend in data was indicated by positive and negative value of Z respectively.
199 At the 5% significance level, the null hypothesis of no trend was rejected if the absolute value of Z was higher than
200 1.96.
201 The magnitude of trend also known as Sen's slope (β) (Sen, 1968) was calculated as

202 $$\beta = median \frac{x_a - x_b}{t_a - t_b} \ldots (7)$$

203 where x_a and x_b denote values in time t_a and t_b respectively.
204 Further, as MK test limited to give monotonic increasing or decreasing trend in the data, to know exact
205 behaviour of the trend, Innovative Trend Analysis (ITA) method was also used. The slope of the ITA was calculated
206 using the following equation (Şen, 2012).

$$s = \frac{2(\bar{x}_2 - \bar{x}_1)}{n} \ldots (8)$$

where, s is the slope of a trend line, $\overline{x_2}$ and $\overline{x_1}$ are the arithmetic mean of the first and second half of the dependent variable respectively, and n is the total number of data used.

2.5 Spatial analysis

Geographic Information System (GIS) is generally accepted as a useful tool for accurate mapping of hydrological parameters such as rainfall and R-factor at catchment and regional scales (Panagos et al., 2015; Raj et al., 2022; Das et al., 2025). For interpolation of point data and preparation of raster maps for rainfall, R-factor and ED, the inverse distance weighting (IDW) interpolation method was used in the present study. The IDW method has been extensively used in hydrological studies because to its simplicity, resilience and easy application. IDW assumes that the distance between two points is inversely proportional to their similarity. Therefore, it is assumed that observations that are closer will have more influence on estimates than observations that are farther away. IDW has been effectively used in a number of studies for the mapping of rainfall and R-factor with reasonable precision (Pinheiro et al., 2018; Dash et al. 2019; Dash et al. 2024a). The combination of GIS with IDW provides an effective and accurate tool for spatial interpolation and display of rainfall, R-factor and ED, which can be used for hydrological and erosion-related studies at catchment and regional scales.

3. Results

3.1 Erosive rainfall and I_{30}-derived R-factor

The magnitude of erosive rainfall varied significantly across AESRs (Table 3). The mean annual erosive rainfall varied from 367.23 mm in AESR-3.0 to 1264.10 mm in AESR-14.2. This indicates that AESR-3.0 is a dry and AESR-14.2 is a wet agro-ecological region. Furthermore, KE can be related to the amount of rainfall. AESR-3.0 (367.23 mm) and ASER-4.1 (393.55 mm) showed lowest mean values of erosive rainfall indicating low rainfall KE and low erosion potential in these relatively dry arid and semi-arid regions. On the other hand, AESR-14.2 (1264.10 mm) recorded the highest mean erosive rainfall, followed by AESR-12.1 (1034.59 mm) and AESR-9.1 (856.58 mm) that are normally characterised by humid or sub-humid climates with high intensity rainfall events. The coefficient of variation (CV) varied from 25.10% in AESR-14.2 to 45.61% in AESR-3.0. The low CV values in sub-humid zones (AESR-9.1, AESR-12.1, and AESR-14.2) indicate low inter-annual variation, implying that erosive rainfall is regular and predictable in the monsoon climate. In contrast, variability was higher in the arid and semi-arid regions (AESR-3.0, AESR-4.1, AESR-4.4, and AESR-5.2), indicating that erosive rainfall in these regions is sporadic, occurring in fewer but more intense rainfall events. This variability can thus be a challenge for the planning of soil and water conservation in arid and semi-arid regions, where years of low erosivity can be followed by extreme erosive storms, causing severe localised erosion

Descriptive statistics of R-factor across AESRs indicate heterogeneity in erosive potential, due to variations in climatic controls. Average annual R-factor values varied from 2,451.83 MJ mm ha^{-1} hr^{-1} yr^{-1} in AESR-3.0 to 10,014.64 MJ mm ha^{-1} hr^{-1} yr^{-1} in AESR-14.2, indicating a gradient from low to extremely high R-factor (Table 3). CV ranged from 34.83% to 67.92% which is consistent with erosive rainfall pattern. Higher CVs were observed in AESR-3.0 (67.92%), AESR-4.1(59.37%), AESR-4.4 (52.82%), and AESR-5.2 (66.14%) indicating high inter-annual variability in rainfall intensity and distribution, whereas regions with low CVs, such as AESR-9.1, AESR-12.1, and AESR-14.2 suggested more stable erosivity regimes.

The box plot of the erosive rainfall and R-factor in different AESRs is shown in Fig. 2, which supports the descriptive analysis of erosive rainfall and R-factor. The boxplot (Fig. 2a) illustrates a high degree of variation in erosive rainfall across AESRs. Regions with low erosive rainfall are AESR-3.0, AESR-4.1, AESR-4.4, and AESR-5.2 having lower medians and relatively dry conditions. But, some regions such as AESR-12.1, AESR-14.2, and AESR-19.2 show higher rainfall and greater variability. Some locations observe the presence of outliers, which are occasional extreme rainfall events that significantly differ from the normal pattern.

Fig. 2b presents the box plot of the R-factor over the AESRs. The AESR-3.0, AESR-4.1, and AESR-5.2 have relatively low median R-factor values indicating low rainfall intensity and infrequent rainfall, resulting in lower erosive potential. In contrast, AESR-9.1, AESR-12.1, and AESR-14.2 show significantly higher R-factor values, with AESR 14.2 displaying the highest median and upper range, indicating that it is the most erosion-prone of the AESRs analysed. The inter-quartile ranges (IQRs) for AESRs, such as 12.1 and 14.2, are wide, suggesting high internal variability in erosive rainfall and R-factor within the zones. However, AESRs like 3.0 and 5.2 exhibit narrower IQRs, indicating more homogeneous erosivity. Tukey's HSD test revealed significant differences in erosive rainfall and R-factor distribution across regions, emphasising the necessity for region-specific erosion assessment and conservation planning.

3.2 Annual R-factor models

Using the calibration data, multiple regression models (linear, exponential, logarithmic, power, and polynomial) were tested to capture the relationship between annual R-factor and respective annual erosive rainfall for all eight locations. The models developed for calculating annual R-factor were compared. Statistical parameters viz. R^2, RMSE, PBIAS, and NSE were used to select the best-fitting model using the standard equations, and the details of best fitted model for each location are shown in Table 4. Out of eight regression models, annual rainfall showed a linear relationship with annual R-factor in AESR-4.4 and AESR-9.1. For the remaining AESRs, power relationship between annual rainfall and annual R-factor was observed (Fig. 3, Table 4). During calibration, the developed model exhibited strong relationship between annual rainfall and annual R-factor for six AESRs (3.0, 4.1, 4.4, 5.2 and 12.1) with R^2 values more than 0.75, except AESR 9.1 and AESR 19.2. The PBIAS values ranged from 0.65% to 9.10%, indicating strong agreement between observed and predicted R-factor values.

The validation data set also showed good predictive performance for almost all the selected AESRs of India. During validation, the annual rainfall-R-factor model developed for AESR-3.0, AESR-4.1, and AESR-12.1 performed well (NSE $\geq$ 0.80; PBIAS within $\pm$10%), indicating strong predictive capability and low systematic bias. The annual

rainfall-R-factor model developed for AESR-14.2 also performed well (NSE = 0.72), while those for AESR-4.4 and AESR-5.2 performed satisfactorily (NSE = 0.65 and 0.61), indicating moderate model reliability despite having high R^2 for AESR-4.4. The developed annual rainfall-R-factor model for AESR-9.0 lies at the lower bound of satisfactory performance (NSE = 0.51), indicating limited predictive robustness. In contrast, for AESR-19.1 the annual rainfall-R-factor model performed poorly, as evidenced by a negative NSE (-0.35), implying that model predictions are inferior to the mean observed rainfall, along with relatively higher PBIAS (13.66%), indicating systematic deviation. Overall, the annual rainfall-R-factor model developed for AESRs performs well, with PBIAS values within the ±10% threshold, confirming low bias and reliably.

3.3 Erosive rainfall and R-factor trend

An analysis of erosive rainfall, and annual R-factor trends revealed that six AESRs especially AESR-3.0, 4.1, 4.4, 5.2, 12.1 and 14.2 showed an increasing trend while other two AESRs (9.1 and 19.2) showed a decreasing trend in both erosive rainfall and annual R-factor (Table 5). The strength of both upward and downward trends ranges from very week to week. The erosive rainfall was observed to increase at the rate of 11.85 mm yr^{-1} for AESR-12.1, but for AESR-14 it was 4.05 mm yr^{-1}. For all other AESRs such as AESR-3.0, AESR-4.1, AESR-4.4, and AESR-5.2, the erosive rainfall is increasing at a rate of 2.20, 2.47, 2.35 and 1.55 mm yr^{-1}, respectively. As MK test is limited to detecting only monotonic trend, ITA method was performed to know comprehensive and complete trend behavior. The results are depicted in Fig 4. The difference in results (Table 5 and Fig. 4) is because the ITA method is more comprehensive, as it can detect both monotonic and non-monotonic trends, and even hidden sub-trends within data. Points above the 1:1 line indicates increasing trend, below the 1:1 line indicates decreasing trend, while on the 1:1 line show, no trend. For all the 8 gauged stations, data points lie both above and below the 1:1 line. With respect to strength of trend, both AESR-4.4 and AESR-14.2 showed moderate increasing trend for erosive rainfall with slope values as 1.40 and 1.46 respectively (Fig. 4a). While AESR-3.0, AESR-4.1 and AESR-19.2 exhibited weak decreasing trend having slope values of 0.93, 0.84 and 0.88, respectively. Other AESRs, such as 5.2, 9.1 and 12.1 showed moderately decreasing trend in erosive rainfall having slope value as 0.68, 0.63, and 0.71, respectively.

With respect to strength of trend for computed I_{30} based annual R-factor, it did not follow the same trend as that of erosive rainfall. Along with AESR-4.4 and AESR-14.2, AESR-3.0 also showed moderate increasing trend for R-factor with slope values as 1.27, 1.16 and 1.06 respectively (Fig. 4b). AESR 12.1 with slope value of 0.91, showed weak decreasing trend. The AESR-4.1, AESR-5.2, AESR-9.1 and AESR-19.2 exhibited moderate decreasing trend having slope values of 0.70, 0.72, 0.67 and 0.73, respectively.

3.4 Spatial variation of annual rainfall and model derived R-factor

Fig. 5. presents the spatial variation of annual rainfall (IMD gridded data) and annual R-factor derived from the developed model (Table 3) using the gridded rainfall data for each AESR. The AESR-3.0 having an arid climate with average annual rainfall between 425 and 674 mm, showed the estimated annual R-factor of 2750 to 4994 MJ mm ha^{-1} hr^{-1} yr^{-1} (Fig. 5a). Similarly, AESR 4.1, a dry semi-arid region had annual rainfall ranging from 420 to 948 mm, and annual R-factor of 3582 to 9400 MJ mm ha^{-1} hr^{-1} yr^{-1} (Fig. 5b). AESR-4.4 and AESR-5.2, with a wet semi-arid climate,

experienced average annual rainfall of 687 to 1077 mm and 637 to 1423 mm, respectively (Fig. 5c, 5d). The estimated annual R-factor ranged from 6425 to 10885 MJ mm ha^{-1} hr^{-1} yr^{-1} for AESR-4.4, while for AESR 5.2, it falls within 5795 to 18325 MJ mm ha^{-1} hr^{-1} yr^{-1} (Fig. 5C, 5D). The sub-humid climatic zones encompassing AESR 9.1, 12.1, and 14.2 experienced average annual rainfall between 676 and 1850 mm, 1069 to 1716 mm, and 700 to 2100 mm, respectively (Figs. 5E, 5F, 5G). The annual R-factor in these regions varied from 7000 to 17766, 6673 to 11454, and 4262 to 19576 MJ mm ha^{-1} hr^{-1} yr^{-1}, respectively. The annual rainfall of AESR 19.2 ranged from less than 1000 mm to more than 4000 mm, and annual R-factor varied between 2548 and 21563 MJ mm ha^{-1} hr^{-1} yr^{-1} (Fig. 5h).

3.5 Monthly and annual erosivity density

The R-factor at any place quantifies the total erosive potential of rainfall, while ED indicates the intensity and aggressiveness of rainfall events relative to the amount of rainfall received. The estimated monthly ED from sub-hourly rainfall data of the gauged stations is presented in Fig. 6. The monthly ED value ranged from 0.1 MJ ha^{-1} hr^{-1} (AESR-19.2 during December) to 12.54 MJ ha^{-1} hr^{-1} (AESR-9.1 during August). All the AESRs observed to have monthly ED values more than 3.0 MJ ha^{-1} hr^{-1} for monsoon months like June, July, August, and September, except AESR-19.1. Similarly, the month of May also experienced ED values greater than 3 MJ ha^{-1} hr^{-1} for all AESR except AESR-19.2. Hence, the ED values across different AESRs show considerable variability, reflecting differences in rainfall intensity and its erosive efficiency across regions.

The mean annual ED varied from 3.34 (AESR-19.2) to 13.83 MJ ha^{-1} hr^{-1} (AESR-5.2) (Fig. 7). Mean annual ED for AESR-3.0 ranged from 6.46 to 7.40 MJ ha^{-1} hr^{-1} and for AESR-4.1, from 8.44 to 9.92 MJ ha^{-1} hr^{-1}. In the semi-arid regions, such as AESR-4.4 and AESR-5.2, annual ED values ranged from 9.35 to 10.10 and 9.06 to 13.83 MJ ha^{-1} hr^{-1}, respectively. The AESR-9.1, AESR-12.1, and AESR-14.2 from sub-humid region recorded annual ED of 8.84 to 9.6, 6.23 to 6.68 and 6.06 to 9.32 MJ ha^{-1} hr^{-1}, respectively. The ED ranged from 3.34 to 5.06 MJ ha^{-1} hr^{-1} in AESR-19.2.

4. Discussions

4.1 Regional differences in erosive rainfall and R-factor

In the present study, both annual erosive rainfall and R-factor varied across the AESRs, with low values in dry arid, and semi-arid AESRs and high values in wet sub-humid, and humid AESRs. Similarly, CV was observed to be higher in arid and semi-arid AESRs compared to wet humid, and sub-humid regions like AESRs 9.1, 12.1, and 14.2, possibly due to local climatic or topographic effects (Dash et al., 2019; Singh & Singh, 2020; Dash et al., 2024b). These findings are in line with earlier reports that noted the R-factor to be higher and more temporally consistent in humid tropics than semi-arid climates (Diodato & Bellocchi, 2010; Singh & Singh, 2020; Dash et al., 2024a). This variability can therefore be a challenge for the planning of soil conservation measures in arid and semi-arid regions, where years of low erosivity can be followed by extreme erosive storms, causing severe localized erosion. High-magnitude and intense erosive rainfall may explain these sub-humid regions' high R-factor pattern (Dash et al., 2019). Due to rainfall heterogeneity, R-factor values vary greatly among the AESRs (Dash et al. 2019; Singh et al., 2020; Dash et al., 2024a),

and demands for region-specific soil erosion management measures. This is especially crucial for high erosivity areas such as AESR-9.1, AESR-14.2, and AESR-12.1, where intense and frequent rainfall events are expected to accelerate soil loss and land degradation processes.

4.2 Implication of rainfall and erosivity trend

Six of the eight AESRs, (3.0, 4.1, 4.4, 5.2, 12.1, and 14.2) showed an increasing trend, whereas two AESRs (9.1 and 19.2) showed a decreasing trend as per the MK test. A similar kind of result was also reported by researchers (Dash et al., 2024a), indicating an increasing trend in annual rainfall (1.24 mm yr^{-1}) for the Eastern Ghats Highland zone of Odisha (data period:1901-2017). However, through ITA method, R-factor was showing increasing trend for three AESRs such as AESRs 3.0, 4.4, and 14.2, in remaining AESRs, the same followed a declining trend. In contrast, a non-significant positive trend in MFI-based annual R-factor (21.46 MJ mm ha^{-1} hr^{-1} yr^{-1}) for Eastern Ghats Highland region of Odisha, which comes under AESR-12.1 was observed (Dash et al., 2024a). The contrasting result may be attributed to different R-factor estimation approaches along with the duration of data. Similarly, a decreasing trend in MFI-based annual R-factor for the Northern Hills (35.61 MJ mm ha^{-1} hr^{-1} yr^{-1}) and the Chhattisgarh Plains (17.55 MJ mm ha^{-1} hr^{-1} yr^{-1}), and an increasing trend for the Bastar Plateau (23.50 MJ mm ha^{-1} hr^{-1} yr^{-1}) in Chhattisgarh state, India, was observed (Dash et al., 2024b) and trend in the annual R-factor in these three agro-climatic zones of Chhattisgarh state was linked with the rainfall trend. There is a likelihood of an increment in the R-factor over western, central and northeastern India (Das & Jain, 2023), which includes AESR 4.1 and 5.2. AESR-4.4, which is a semi-arid region and is showing an increasing trend both in erosive rainfall and annual R-factor, indicates high-intensity rainfall, and therefore, more focus should be given on soil conservation. Similarly, AESR-14.2, which is under a sub-humid region showing an increasing trend both in erosive rainfall and annual R-factor. Therefore, the region may witness amplifying soil detachment and transport due to humid environment promoting rapid runoff. The Himalayan regions, where AESR 14.2 is located, fall within the broader landslide-prone belt identified in the Landslide Atlas of India; the increasing trend of erosive rainfall and R-factor can significantly aggravate slope instability and mass erosion. AESR 3.0 is an arid region, which showed decreasing erosive rainfall trend with increasing R-factor trend, indicating more intense rainfall events, which may be due to convective activities producing short-duration, high-intensity downpours delivering greater KE, even though when total erosive rainfall declines. The situation may enhance erosional activity in this region, as the region is characterized by prolonged dry spells which may weaken soil structure, reduce organic matter, and diminish vegetation cover, leaving the soil highly vulnerable to erosion. The anthropogenic activities such as deforestation, agricultural expansion may further reduce ground cover, and magnify the erosion.

4.3 Spatial patterns and controls of R-factor and ED

The model derived R-factor and ED were mapped for the selected 8 AESRs of India, and showed a spatial variation across the region. The MFI-based annual R-factor for Suketi river catchment in Mandi district of Himachal Pradesh (AESR-14.2) ranged from 146.82 to 2007.76 MJ mm ha^{-1} hr^{-1} yr^{-1}, with a mean value of 775.90 MJ mm ha^{-1} hr^{-1} yr^{-1} (Singh & Singh, 2020). A global R-factor map, showed the average annual R-factor for India as 3848.97 MJ mm ha^{-1} hr^{-1} yr^{-1}, while the maximum value reported as12749 MJ mm ha^{-1} hr^{-1} yr^{-1} (Panagos et al., 2017). Based on I_{60} method,

the average R-factor for India was estimated as 1200 MJ mm ha^{-1} hr^{-1} yr^{-1} (Raj et al., 2022). The minimum and maximum values were 8.10 MJ mm ha^{-1} hr^{-1} yr^{-1} for the Shahi Kangri mountain region of Ladakh and 23909.21 MJ mm ha^{-1} hr^{-1} yr^{-1} for the Laitknsew and Cherrapunji region of East Khasi Hills in Meghalaya state. Annual average I_{30} derived R-factor for AESR-19.2 ranged between 6,979 to 22,901 MJ mm ha^{-1} hr^{-1} yr^{-1} with a mean value of 13,460 MJ mm ha^{-1} hr^{-1} yr^{-1} (Nandgude et al., 2013). The difference in results for AESR-19.2 is due to the method and the duration of data used for the estimation of R-factor. This is on top of the fact that both erosive rainfall and R-factor are decreasing over time.

Table 6 presents a comparative analysis of the annual R-factors calculated at the eight AESRs in the present study against the national-scale estimates provided by previous researchers. The R-factor maps developed by researchers (Raj et al., 2022; Das et al., 2022; Das et al., 2025) were geo-referenced and digitized, enabling the extraction of location-specific values through spatial superposition. The results indicate a consistent influence of temporal rainfall resolution on R-factor estimation. The IMDAA hourly dataset yielded lower annual R-factor values across all AESRs. A similar trend of underestimation was also observed with IMERG sub-hourly data for all eight AESRs. However, for low rainfall regions, (AESR 3.0, 4.1, and 4.4), R-factors calculated from hourly IMD data were at par with sub-hourly estimates, suggesting that hourly temporal resolution can be considered as an option for estimation of R-factor in low-intensity rainfall regions. This agreement was not consistent in higher-rainfall regions, where hourly data underestimated R-factors in AESRs 9.1, 12.1, and 14.2 but overestimated them in AESR-19.2. These variations highlight the limitation of hourly resolution in capturing short-duration, high-intensity rainfall peaks, which substantially influence erosive energy and R-factor estimation. It also highlights the sensitivity of erosivity calculations to temporal resolution in humid climates.

Erosivity density also varies a lot, spatially and temporally. The mean monthly ED for India ranged from 0.81 (February) to 2.34 MJ ha^{-1} hr^{-1} (July) (Das et al., 2022). Higher ED value (>1 MJ ha^{-1} hr^{-1}) indicates occurrence of high R-factor from a certain amount of rainfall (Das et al., 2022). ED values more than 3 MJ ha^{-1} hr^{-1} significantly contributes to the flood risk and the higher runoff prediction (Dabney et al., 2011). The monthly ED was 0.02 MJ ha^{-1} hr^{-1} in April to 0.78 MJ ha^{-1} hr^{-1} in July for Suketi river catchment, Mandi district, Himachal Pradesh (AESR-14.2) (Singh & Singh, 2020), while monthly ED values ranged from 2.9 to 5.4 MJ ha^{-1} hr^{-1} in Eastern Ghats Highland, Odisha (AESR-12.1) (Dash et al., 2019). The ED values less than 3 MJ ha^{-1} hr^{-1} were associated with low rainfall intensity (<6 mm hr^{-1}), whereas higher rainfall intensities such as 18 to 30 mm hr^{-1} and greater than 30 mm hr^{-1} experienced ED values more than 9 and 15 mm hr^{-1}, respectively (Dash et al., 2019). Therefore, for monsoonal climate like India, the relationship between rainfall intensity and ED for all agro-ecological or agro-climatic regions need to be established. Further, the variation in ED values of India as reported by Das et al. (2022) and Das et al. (2025) may be due to derivation of R-factor from different data sources and not considering direct measurements of rainfall intensity (sub-hourly intensity data) and exact KE of individual storm events.

The mean value of annual ED was 1.85 MJ ha^{-1} hr^{-1} in India with a range of 0.26-7.05 MJ ha^{-1} hr^{-1} (Das et al., 2022). Similarly, annual ED ranged from 1.01 to 2.85 MJ ha^{-1} hr^{-1} with an average value of 1.92 MJ ha^{-1} hr^{-1} for Suketi river catchment of western Himalayan region in India (Singh & Singh, 2020). In the present study, the spatial variation of ED values for various AESRs was determined by employing R-factor calculated from IMD gridded daily rainfall data

using empirical relationships, instead of direct measurements of rainfall intensity (sub-hourly intensity data). Thus, the ED calculated, is the relative erosive efficiency of rainfall in terms of modelled erosivity, not the actual KE of individual storm events. This limitation is relevant in the interpretation of the results, especially for areas where high-intensity short-duration storms are not necessarily captured by the daily rainfall data. But the ED patterns do offer meaningful insight. AESRs 12.1, 14.2 and 19.2, in particular, are characterised by high annual rainfall and relatively low to moderate values of ED. This implies that, despite receiving considerable rainfall, these regions are likely to receive it over longer periods or at relatively low intensity, thus resulting in lower erosive efficiency per unit of rainfall. On the other hand, AESRs like 5.2, 4.4 and 4.1 have higher ED values, indicating that even under conditions of relatively low to moderate total rainfall, the rainfall events are more effective in producing erosive energy. The analysis therefore suggests that high rainfall does not automatically mean high ED, particularly when the R-factor is estimated using empirical equations and daily rainfall inputs. The variations in ED observed across AESRs reflect differences in the distribution pattern of rainfall and the limitations of the input data, rather than the exact dynamics of the storm intensity. However, even when derived from gridded datasets, ED is a useful comparative indicator to identify regions where rainfall is relatively more erosive and can help prioritise soil conservation efforts at the regional scale.

4.4 Soil and water conservation planning

Soil and water conservation strategies at different AESRs should be formulated according to their specific climatic regimes, soil characteristics and rainfall erosivity patterns (Fig. 8). In dry AESR 3.0 (Deccan Plateau) having low rainfall (300-500 mm), short LGP and mixed red and black soils with weak upward trend in erosive rainfall and annual ED values > 3 MJ ha^{-1} hr^{-1} emphasis needs to be given to in-situ moisture conservation practices like contour farming, compartment bunding, mulching, farm ponds for supplemental irrigation and ground water recharge structures like check dams and percolation tanks (Naik et al., 2021). In semi-arid AESRs 4.1, 4.4 and 5.2, characterised by moderate rainfall (500-1000 mm) and deep alluvial or black soils, conservation measures should focus on efficient water management and runoff control through graded bunding, broad-bed and furrow systems, contour trenching and small water harvesting structures, supplemented by conservation agriculture practices and agro-forestry (Singh et al., 2023). However, in the sub-humid AESR-9.1, despite the presence of deep alluvial soils and relatively high rainfall, the erosivity is showing a weak declining trend. In such a situation, priority should be given to proper drainage, flood control and conservation tillage to reduce waterlogging and maintain soil structure (Panwar et al., 2023).

However, AESR-12.1 consisting of Eastern Ghats and Dandakaranya region receives high rainfall (1000-1600 mm) with increasing R-factor and requires integrated watershed management approaches like graded bunding, contour trenching, afforestation and gully control measures to combat substantial runoff and soil loss (Madhu et al., 2016; Dash et al., 2023; Dash et al., 2024a,b). Because of the steep and fragile topography of the Himalayas in the AESR-14.2 region, substantial methods of soil stabilisation are required to minimise landslides and erosion under high rainfall circumstances. Bench terracing, bioengineering measures, controlled grazing and afforestation are some of the soil stabilisation strategies. Similarly, the humid Western Ghats AESR-19.2, with more than 2000 mm of rainfall, needs high vegetative cover, contour bunding, staggered trenches and drainage line treatments for regulating the excess runoff and preventing severe soil erosion (Kanan et al., 2021). The choice and application of conservation measures

should, in general, be consistent with regional hydro-climatic conditions, soil characteristics and observed erosivity trends, leading to sustainable management of land and water resources.

5. Conclusions

It is necessary to develop the location-specific rainfall-R-factor models due to the high spatial variation of rainfall and limited availability of sub-hourly rainfall data. The present study was carried out to develop the annual rainfall-R-factor model for 8 AESRs of India using sub-hourly rainfall data. The annual rainfall-R-factor model developed for AESR-3.0, AESR-4.1 and AESR-12.1 exhibit very good performance, while model developed for AESR-14.2 shows good performance, and the model developed for AESR-4.4 and AESR-5.2 fall within satisfactory category. The relationship of annual rainfall with annual R-factor was found linear for AESR-4.4 and AESR-9.1 while remaining AESRs exhibited power relationship. I_{30}-based average annual R-factor values varied from 2,451.83 MJ mm ha^{-1} hr^{-1} yr^{-1} in AESR-3.0 to 10,014.64 MJ mm ha^{-1} hr^{-1} yr^{-1} in AESR-14.2, corresponding to a gradient from a relatively low to an extremely high erosivity. Further, AESRs-3.0, 4.1, 4.4, 5.2, 12.1, and 14.2 showed increasing trend while other two AESRs (9.1 and 19.2) showed downward trend for both erosive rainfall and annual R-factor. The comparison of R-factor values estimated with sub-hourly data shows underestimation of annual R-factor values in all AESRs calculated with IMDAA hourly dataset and IMERG sub-hourly data. However, for low rainfall regions, hourly IMD data were comparable to sub-hourly estimates indicating that hourly temporal resolution can be considered as an alternative option for estimation of R-factor in low-intensity rainfall regions. All the AESRs found to have monthly ED values more than 3.0 MJ ha^{-1} hr^{-1} for monsoon months indicating severity of water induced erosion in India. Thus, planning of soil and water conservation measures in different AESRs of India should be specific to their respective climatic regimes, soil characteristics and rainfall erosivity patterns.

References

Adhikary, P.P., Hombegowda, H.C., Barman, D., & Madhu, M. (2018). Soil and onsite nutrient conservation potential of aromatic grasses at field scale under a shifting cultivated, degraded catchment in Eastern Ghats, India. *International Journal of Sediment Research,* 33(3), 340-350. https://doi.org/10.1016/j.ijsrc.2018.01.002

Bezak, N., Borrelli, P., & Panagos, P. (2022). Exploring the possible role of satellite-based rainfall data in estimating inter- and intra-annual global rainfall erosivity. *Hydrology and Earth System Sciences,* 26, 1907-1924.

Brown, L.C., & Foster, G.R. (1987). Storm erosivity using idealized intensity distribution. *Transaction of the America Society of Agricultural Engineers,* 30(2), 379-386.

Dabney, S.M., Yoder, D.C., Vieira, D.A.N., & Bingner, R.L. (2011). Enhancing RUSLE to include runoff-driven phenomena. *Hydrological Processes,* 25(9), 1373-1390.

Daoud, N.B., Daoudi, L., Rachdane, M., Gourfi, A., & Saidi, M.E. (2024). Suitability of satellite-based rainfall products for estimating rainfall erosivity in areas with contrasted climate and terrain properties*:* Example of west-central Morocco. *Journal of Earth System Science,* 133, 78**.** DOI: 10.1007/s12040-024-02287-2.

Das, S., & Jain, M.K. (2023). Unravelling the future changes in rainfall erosivity over India under shared socio-economic pathways. *Catena,* 232. https://doi.org/10.1016/j.catena.2023.107417.

Das, S., Jain, M.K., & Gupta, V. (2022). A step towards mapping rainfall erosivity for India using high-resolution GPM satellite rainfall products. *Catena* 212,106067. https://doi.org/10.1016/j.catena.2022.106067.

Das, S., Jain, M.K., Auerswald, K., de Mello, C.R., & Molnar, P. (2025). Identifying monthly rainfall erosivity patterns using hourly rainfall data across India. *Scientific Reports,* 15, 27940.

Dash, Ch. J., Adhikary, P.P., Beer, K., Madhu, M., Sahoo, D.C., & Naik, B.S. (2020). Rainfall, temperature and reference evapotranspiration trend in the context of climate change over undivided Koraput district, Odisha, India. *Indian Journal of Soil Conservation*, 75(2), 174-183.

Dash, Ch. J., Adhikary, P.P., Das, N.K., Alam, N.M., Mandal, U., & Mishra, P.K. (2018). Comparison of rainfall kinetic energy-intensity relationships for Eastern Ghats Highland region of India; *Natural Hazards,* 93, 547-558.

Dash, Ch. J., Das, N.K., & Adhikary, P.P. (2019). Rainfall erosivity and erosivity density in Eastern Ghats highland of east India. *Natural Hazards,* 97(2), 727-746. https://doi.org/10.1007/s11069-019-03670-9.

Dash, Ch. J., Lenka. J., Hombegowda, H.C., Bishnoi, R., Yadav, P., Mandal, D., Dogra, P., Kumar, G., Kaushal, R., Roy, T., Islam, S., & Madhu, M. (2023). Soil erosion status, priority treatment areas and conservation measures for different districts of Odisha. ICAR-Indian Institute of Soil and Water Conservation, Dehradun, Uttarakhand, India.

Dash, Ch. J., Shrimali, S.S., Madhu, M., Kumar, R., & Adhikary, P.P. (2024a). Unveiling rainfall and erosivity dynamics in Odisha's varied agro-climatic zones for sustainable soil and water conservation planning. *Theoretical and Applied Climatology,* 155**,** 7557-7574.

Dash, Ch. J., Yadav, P., Kumar, R., Patra, S.S., Hombegowda, H.C., & Adhikary, P.P. (2024b). Assessing rainfall patterns, erosivity dynamics, and sustainable soil and water management strategies across agro-climatic zones of Chhattisgarh, India. *Indian Journal of Soil Conservation,* 52(2), 1-11.

Diodato, N., & Bellocchi, G. (2010). MedREM, a rainfall erosivity model for the Mediterranean region. *Journal of Hydrology,* 387(1), 119-127.

Fenta, A.A., Tsunekawa, A., Haregeweyn, N., Yasuda, H., Tsubo, M., Borrelli, P., Kawai, T., Belay, A.S., Ebabu, K., Berihun, M.L., Sultan, D., Setargie, T.A., Elnashar, A., Arshad, A., & Panagos, P. (2024) An integrated modeling approach for estimating monthly global rainfall erosivity. *Scientific Reports,* 14, 8167.

Fenta, A.A., Yasuda, H., Haregeweyn, N., Belay, A.S., Hadush, M., Gebremedhin, M.A., Mekonnen, M., & Panagos, P. (2023). Improving satellite-based global rainfall erosivity estimates by merging with gauge data. *Journal of Hydrology,* 622, 129731.

Foster, G.R., Yoder, D.C., Weesies, G.A., McCool, D.K., McGregor, K.C., & Bingner, R. (2008). Draft user's guide, revised 15 universal soil loss equation version 2 (RUSLE-2), Washington, DC.

Goswami, B.N., Venugopal, V., Sengupta, D., Madhusoodanan, M.S., & Xavier, P.K. (2006). Increasing trend of extreme rain events over India in a warming environment. *Science,* 314(5804), 1442-1445. https://doi.org/10.1126/science.1132027.

Gu, Z., Feng, D., Duan, X., Gong, K., Li, Y., & Yue, T. (2020). Spatial and temporal patterns of rainfall erosivity in the Tibetan Plateau. *Water,* 12, 200.

Gu, Z., Li, Y., Huang, S., Yao, C., Ji, K., Feng, D., Yi, Q., & Li, P. (2025). Assessment of erosive rainfall and its spatial and temporal distribution characteristics: Case study of Henan Province, Central China. *Water,* 7, 62.

Hernando, D., & Romana, M.G. (2015) Estimating the rainfall erosivity factor from monthly precipitation datas in the Madrid regions (Spain). *Journal of Hydrology Hydromech,* 63(1), 55-62, DOI: 10.1515/johh-2015-0003.

Hombegowda, H.C., Kannan, K., Kumar, G., Mandal, D., Dogra, P., Kaushal, R., & Madhu, M. (2021). Soil erosion status, priority treatment areas and conservation measures for different districts of Kerala. ICAR-Indian Institute of Soil and Water Conservation, Dehradun, Uttarakhand, India.

IPCC (2023). *Climate change 2021: The physical science basis. Working Group I contribution to the Sixth Assessment Report of the Intergovernmental Panel on Climate Change*. Cambridge University Press. https://doi.org/10.1017/9781009157896.

Kannan, K., Hombegowda, H.C., Kumar, G., Mandal, D., Dogra, P., Kaushal, R. & Madhu M (2021) Soil erosion status, priority treatment areas and conservation measures for different districts of Tamil Nadu, ICAR-Indian Institute of Soil and Water Conservation, Dehradun, Uttarakhand.

Lee, J.H., & Heo, J.H. (2011). Evaluation of estimation methods for rainfall erosivity based on annual precipitation in Korea. *Journal of Hydrology,* 409**,** 30-48, https://doi.org/10.1016/j.jhydrol.2011.07.031.

Lee, Ming-His., & Hsu, I-Ping. (2021). Estimation of the annual rainfall erosivity index based on hourly rainfall data in a tropical region. *Soil and Water Research,* 16(2), 74-84. doi: 10.17221/25/2020-SWR.

Liu, B., Tao, H., Song, C., Guo, B., Shi, Z., Zhang, C., Kong, B., & He, B. (2013) Temporal and spatial variations of rainfall erosivity in china during 1960 to 2009. *Geographical Research,* 32 (2), 245-256, https://doi.org/10.11821/yj2013020005.

Lobo, G.P., & Bonilla, C.A. (2015). Sensitivity analysis of kinetic energy-intensity relationships and maximum rainfall intensities on rainfall erosivity using a long-term precipitation data set. *Journal of Hydrology,* 527**,** 788-793.

Machiwal, D., Santra, P., Meena, H.M., & Singh, A. (2025). Impact of time resolution of rainfall measurement on erosivity factor in arid region of India. *Annals of Arid Zone,* 64(4), 537-554. https://doi.org/10.56093/aaz.v64i4.168282.

Madhu, M., Naik, B.S., Jakhar, P., Hombegowda, H.C., Adhikary, P.P., Gore, K.P., Barman, D., & Naik, G.B. (2016). Comprehensive impact assessment of resource conservation measures in watershed of eastern region of India. *Journal of Environmental Biology,* 37, 391-398.

Mann, H.B. (1945). Nonparametric tests against trend. *Econometrica,* 13, 245.

Moriasi, D.N., Arnold, J.G., Van Liew, M.W., Bingner, R.L., Harmel, R.D., & Veith, T.L. (2007). Model evaluation guidelines for systematic quantification of accuracy in watershed simulations. *American Society of Agricultural and Biological Engineers,* 50(3)**,** 885-900.

Murthy, R.S. & Pandey, S. (1978). Delineations of agro-ecological regions of India. In Paper presented in Commission V, 11th Congress of Inter-departmental Science Students' Society, Edmonton, Canada, 19-27 June 1978.

572 Naik, B.S., Ramesha, M.N., Prabhavathi, M., Dupdal, R., Ravi, K.N., Kumar, G., Mandal, D., Dogra, P., Kaushal, R.,
573 & Madhu, M. (2021). Soil erosion status, priority treatment areas and conservation measures for different
574 districts of Karnataka. ICAR-Indian Institute of Soil and Water Conservation, Dehradun, Uttarakhand, India.
575 Nandgude, S., Shinde, V., Mahale, D., & Singh, M. (2013). Synthesis of rainfall characteristics for predicting the
576 erosivity pattern of Wakavali region in Maharashtra, India. *Journal of Hydrologic Engineering,* 18(1), 92-98.
577 Nash, J.E., & Sutcliffe, J.E. (1970). River flow forecasting through conceptual model. *Journal of Hydrology,* 10, 282-
578 290.
579 Panagos, P., Ballabio, C., Borrelli, P., & Meusburger, K. (2016). Spatio-temporal analysis of rainfall erosivity and
580 erosivity density in Greece, *Catena,* 137,161-172.
581 Panagos, P., Ballabio, C., Borrelli, P., Meusburger, K., Klik, A., Rousseva, S., Tadić, M.P., Michaelides, S.,
582 Hrabalíková, M., Olsen, P., Aalto, J., Lakatos, M., Rymszewicz, A., Dumitrescu, A., Beguería, S., & Alewell,
583 C. (2015). Rainfall erosivity in Europe. *Science of The Total Environment,* 511, 801-814.
584 Panagos, P., Borrelli, P., Meusburger, K., *et al.* (2017). Global rainfall erosivity assessment based on high-temporal
585 resolution rainfall records. *Scientific Reports,* 7(1), 4175. https://doi.org/10.1038/s41598-017-04282-8.
586 Panwar, P., Premi, O.P., Pal, S., Dogra, P., Mandal, D., Kumar, G., Kaushal, R., Roy, T., Islam, S., & Madhu, M.
587 (2023). Soil erosion status, priority treatment areas, conservation measures for different districts of Punjab.
588 ICAR-Indian Institute of Soil and Water Conservation, Dehradun, Uttarakhand, India.
589 Pinheiro, A.G., Souza, T.E., Montenegro, S.M., Montenegro, A.A., & Guerra, S.M. (2018). Rainfall pattern and
590 erosion potential in the physiographic regions of the state of Pernambuco, Brazil. *Revista Brasileira de*
591 *Engenharia Agrícola e Ambiental,* 22(12), 849-853.
592 Planning Commission of India (1990). Agro-climatic Zones of India, Annual Report 1989-90, Government of India,
593 pp. 39-40.
594 Raj, R., Saharia, M., Chakma, S., & Rafieinasab, A. (2022). Mapping rainfall erosivity over India using multiple
595 precipitation datasets. *Catena,* 214**,** 106256.
596 Rambabu, Tejwani, K.G., Agarwal, M.C., & Chandra, S. (1978) Rainfall erosion potential and iso-erodent map of
597 India. Bulletin No. 2. Central Soil and Water Conservation Research and Training Institute, Dehradun, India.
598 Sehgal, J., Mandal, D.K., Mandal, C. & Vadivelu, S. (1992). Agroecological regions of India, 2nd Edn, NBSS&LUP,
599 Publ. No. 24, National Bureau of Soil Survey and Land Use Planning, Nagpur, p. 130.
600 Sehgal, J.L., Mandal, D.K., & Mandal, C. (1996). Agro-ecological sub-regions map of India, National Bureau of Soil
601 Survey and Land Use Planning, Nagpur, India.
602 Sen, P. K. (1968). Estimates of the regression coefficient based on Kendall's Tau. *Journal of the American Statistical*
603 *Association*, *63*(324), 1379-1389. https://doi.org/10.1080/01621459.1968.10480934.
604 Şen, Z. (2012). An Innovative Trend Analysis Methodology. *Journal of Hydrologic Engineering,* 17(9), 1042-1046.
605 https://doi.org/10.1061/(ASCE)HE.1943-5584.0000556.
606 Singh, A.K., Dakshnamoorthy, D., Singh, G., Jinger, D., Mandal, D., Dogra, P., Kumar, G., Kaushal, R., Roy, T.,
607 Islam, S., & Madhu, M. (2023). Soil erosion status, priority treatment areas, conservation measures for different
608 districts of Gujarat, ICAR-Indian Institute of Soil and Water Conservation, Dehradun, Uttarakhand, India.

Singh, J., & Singh, O. (2020). Assessing rainfall erosivity and erosivity density over a western Himalayan catchment, India. *Journal of Earth System Science,* 129**,** 97.

Thakur, M.K., Kumar, T.V.L., Narayanan, M.S., Kundeti, K.R., & Barbosa, H. (2020). Analytical study of the performance of the IMERG over the Indian landmass. *Meteorological Applications,* 27, 1-11.

Tiwari, H., Rai, S. Pd., Kumar, D., & Sharma, N. (2016). Rainfall erosivity factor for India using modified Fourier index. *Journal of Applied Water Engineering and Research*, *4*(2), 83-91. https://doi.org/10.1080/23249676.2015.1064038.

Tu, A., Xie, S., Li, Y., Liu, Z., & Shen, F. (2023). Effect of fixed time interval of rainfall data on calculation of rainfall erosivity in the humid area of south China. *Catena,* 220, 106714.

Wischmeier, W.H., & Smith, D.D. (1978). Predicting rainfall erosion. USDA Agriculture Handbook No. 537. Washington, DC.

Yang, X.H., & Yu, B.F. (2015). Modelling and mapping rainfall erosivity in New South Wales, Australia. *Soil Research,* 53(2), 178-189.

Yin, S., Xie, Y., Nearing, M.A., & Wang, C. (2007). Estimation of rainfall erosivity using 5- to 60-min fixed-interval rainfall data from China. *Catena,* 70(3), 306-312.

Table 1 Overview of the agro-ecological characteristics of the selected agro-ecological sub-regions (AESRs) of India included in the present study.

AESR	Name	Area (M ha)	Eco-system	Soil type	Rainfall (mm)	LGP (Days)	Mean temperature (°C)	Major state covered
3.0	Deccan Plateau	4.85	Arid	Mixed red and black	300-500	60-90	25-28	AP, KN
4.1	North Punjab Plain / Ganga-Yamuna Doab and Rajasthan Uplands	11.51	Semi-arid (dry)	Deep loamy alluvium	500-1000	90-120	24-27	GJ, RJ, UP, MP, HR, PB
4.4	Madhya Bharat Plateau and Bundelkhand Uplands	5.15	Semi-arid (moist)	Mixed red and black	500-1000	120-150	24-27	MP, UP, RJ
5.2	Central Highlands / Malwa Plateau and Vindhyas	13.63	Semi-arid (moist)	Deep black	500-1000	120-150	24-28	GJ, MP
9.1	Northern Plain / Rohilkhand type	4.20	Sub-humid	Deep alluvium	1000-1200	120-150	24-27	Bihar, UP, Punjab
12.1	Garjat Hills / Dandakaranya / Eastern Ghats	17.72	Sub-humid (moist)	Deep loamy, red and lateritic	1000-1600	180-210	24-27	OD, WB, JH, CH, TG, MH
14.2	South Kashmir and Kumaun Himalayas	9.51	Sub-humid (moist)	Brown forest andpodzolic	1000-2000	180-210	15-20	J&K, HP, UP, UK
19.2	Central and South Sahyadris	6.64	Humid	Red, and lateritic	>2000	210-240	25-28	KL, GA, MH, GJ, TN,Daman & Diu,

AP: Andhra Pradesh, CH: Chhattisgarh; GA: Goa; GJ: Gujarat, HP: Himachal Pradesh, HR: Haryana; J&K: Jammu and Kashmir, JH: Jharkhand, KN: Karnataka, KL: Kerala; MH: Maharashtra, MP: Madhya Pradesh, OD: Odisha; PB: Punjab; RJ: Rajasthan, TN: Tamil Nadu, TG: Telangana; UK: Uttarakhand, UP: Uttar Pradesh, WB: West Bengal

Table 2. Temporal coverage of the rainfall dataset and the number of rainfall events used to develop the rainfall erosivity (R-factor) model for the selected agro-ecological sub-regions (AESRs) of India.

AESR	Station name	Data duration	Missing year	No. of events > 12.6 mm
ASER-3.0	Bellary	1977-2017	2018-20	558
ASER-4.1	Agra	1969-2020	1974-79, 1983-84, 1992	560
AER-4.4	Datia	2002-2020	-	271
AER-5.2	Kota	1956-2020	1974, 1987, 1991-92	956
AER-9.1	Chandigarh	1997-2020	-	549
AER-12.1	Koraput	1994-2020	-	824
AER-14.2	Dehradun	1993-2020	-	684
AER-19.2	Udhagamandalam	1997-2020	-	704

Table 3. Descriptive statistics of erosive rainfall characteristics and I_{30}-derived rainfall erosivity (R-factor) for gauged stations across the selected agro-ecological sub-regions (AESRs) of India.

AESR	**Minimum**	**Maximum**	**Mean**	**SD**	**CV (%)**	**Minimum**	**Maximum**	**Mean**	**SD**	**CV (%)**
	Erosive rainfall (mm)					R-factor (MJmm/ha/hr/yr)				
ASER-3.0	114.50	834.40	367.23	167.48	45.61	349.85	8672.59	2451.83	1665.17	67.92
ASER-4.1	59.90	858.40	393.55	164.89	41.90	368.25	9397.58	3254.49	1932.21	59.37
AER-4.4	167.20	841.47	492.09	191.81	38.98	1471.12	9626.01	4448.68	2349.68	52.82
AER-5.2	32.28	1120.40	477.84	209.69	43.88	26.16	10110.88	3842.00	2541.28	66.14
AER-9.1	575.00	1451.90	856.58	217.13	25.35	3539.69	13862.48	8047.95	2803.06	34.83
AER-12.1	256.40	1657.10	1034.59	322.73	31.19	1300.8	12587.38	6541.99	2557.42	39.09
AER-14.2	699.86	2213.20	1264.10	317.32	25.10	3585.33	16879.98	10014.64	3531.94	35.27
AER-19.2	379.10	1417.30	804.31	287.39	35.73	765.51	6048.28	2788.78	1358.54	48.71

SD: Standard deviation; CV: Coefficient of variation

Table 4. Best-fit empirical rainfall erosivity (R-factor) models developed from rainfall characteristics and their performance statistics, across the selected agro-ecological sub-regions (AESRs) of India.

AESR	Model (Type)	Model development			Model validation			
		R^2	RMSE	PBIAS (%)	R^2	NSE	RMSE	PBIAS (%)
ASER-3.0	$R_a=0.885\times P_a^{1.324}$ (Power)	0.83	465.16	0.65	0.80	0.82	416.68	3.13
ASER-4.1	$R_a=2.352\times P_a^{1.208}$ (Power)	0.81	390.35	4.14	0.78	0.80	411.65	4.66
AER-4.4	$R_a=11.43P_a-1424.1$ (Linear)	0.88	987.23	9.10	0.84	0.65	1124.35	9.10
AER-5.2	$R_a=0.089\times P_a^{1.705}$ (Power)	0.79	1276.59	3.93	0.73	0.61	1288.67	4.51
AER-9.1	$R_a=10.04Pa-811$ (Linear)	0.61	1356.89	6.88	0.51	0.51	1490.4	9.21
AER-12.1	$R_a=2.257\times P_a^{1.145}$ (Power)	0.84	1048.85	1.28	0.77	0.82	1372.65	1.60
AER-14.2	$R_a=0.463\times P_a^{1.390}$ (Power)	0.73	1552.36	7.50	0.68	0.72	1805.18	8.19
AER-19.2	$R_a=0.713\times P_a^{1.231}$ (Power)	0.68	946.88	6.71	0.49	-0.35	1408.04	13.66

P_a: Annual rainfall, R_a: Annual R-factor

Table 5. Mann–Kendall trend statistics (Tau), Sen's slope estimates, and corresponding temporal trends in erosive rainfall and I_{30}-derived rainfall erosivity (R-factor) across the selected agro-ecological sub-regions (AESRs) of India.

AESRs	Duration	MK Tau		Sen's slope		Trend		Change year	
		Erosive rainfall	R-factor	Erosive rainfall	R-factor	Erosive rainfall	R-factor	Erosive rainfall	R-factor
AER-3.0	1977-2017	0.13	0.20	2.20	32.58	Very weak upward	Weak upward	2007	2007
AER-4.1	1969-2020	0.12	0.02	2.47	5.88	Very weak upward	Very weak upward	1987	2010
AER-4-4	2002-2020	0.01	0.10	2.35	29.46	Very weak upward	Very weak upward	2013	2008
AER-5.2	1956-2020	0.10	0.06	1.55	13.61	Very weak upward	Very weak upward	1966	1966
AER-9.1	1997-2020	-0.08	-0.05	-5.15	-24.13	Very weak downward	Very weak downward	2014	2004
AER-12.1	1994-2020	0.20	0.18	11.85	95.85	Weak upward	Very weak upward	2011	2015
AER-14.2	1993-2020	0.12	0.08	4.05	49.78	Very weak upward	Very weak upward	2009	2009
AER-19.2	1997-2020	-0.09	-0.13	-7.10	-34.14	Very weak downward	Very weak downward	2011	2011

Table 6. Comparison of rainfall erosivity (R-factor) estimates obtained in the present study with those reported in previous studies.

AESR	Sub-hourly data (Present study)	Hourly IMDAA data (Raj et al., 2022)	IMERG sub-hourly data (Das et al., 2022)	Hourly IMD data Das et al., 2025
	R-factor (MJ mm ha^{-1} hr^{-1} yr^{-1})			
ASER-3.0	2451.83	0-1500	300-700	2500-3000
ASER-4.1	3254.49	0-1500	700-1300	3000-5000
AER-4.4	4448.68	0-1500	1300-1500	3000-5000
AER-5.2	3842.00	0-1500	1500-2500	5000-7000
AER-9.1	8047.95	0-1500	1500-2500	3000-5000
AER-12.1	6541.99	3000-4500	2500-3400	5000-7000
AER-14.2	10014.64	4500-6000	2500-3400	5000-7000
AER-19.2	2788.78	0-1500	1500-2500	5000-7000

1

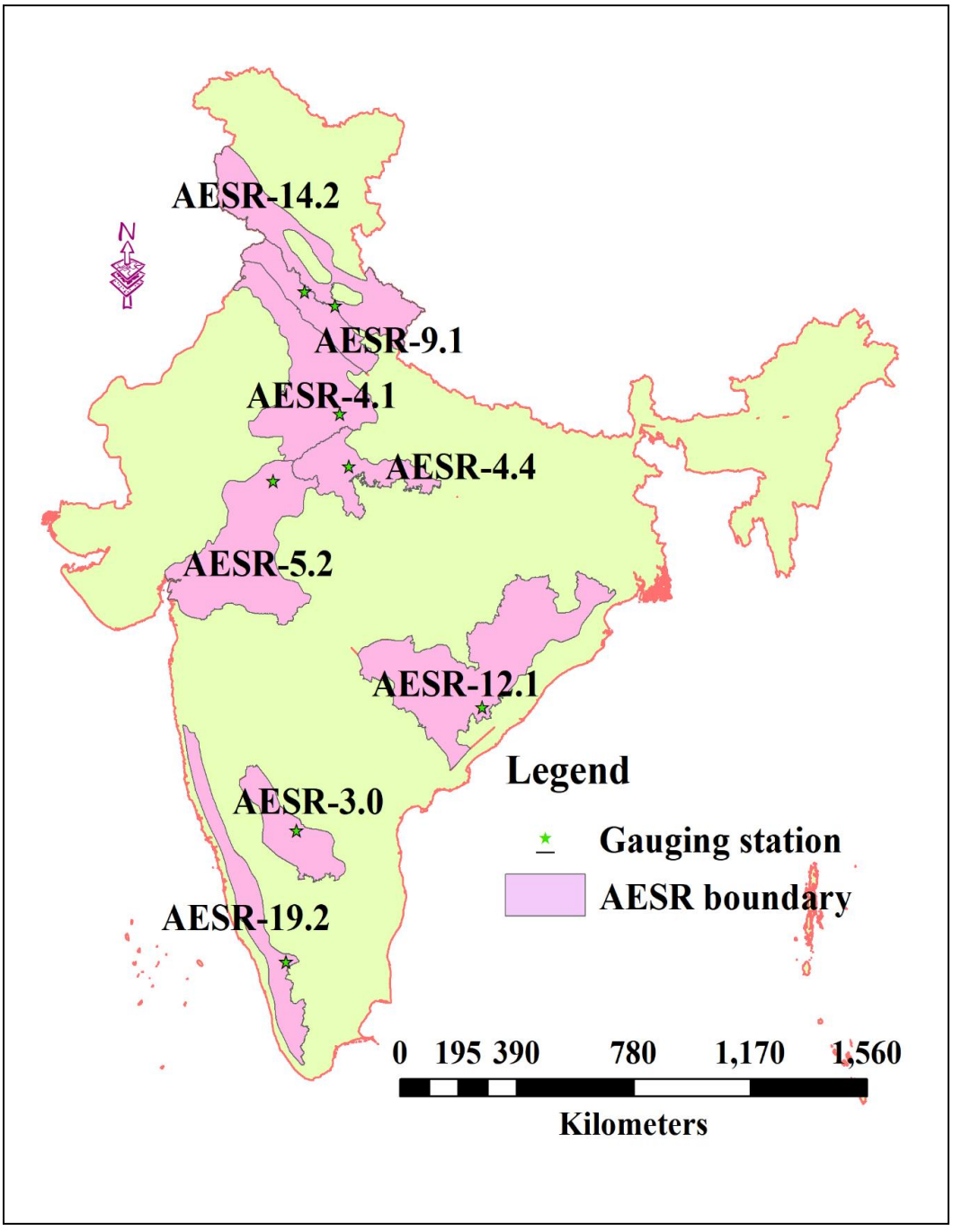

Figure 1. Location map of the study area showing the selected agro-ecological sub-regions (AESRs) of India and the spatial distribution of recording rain gauge stations used in the study.

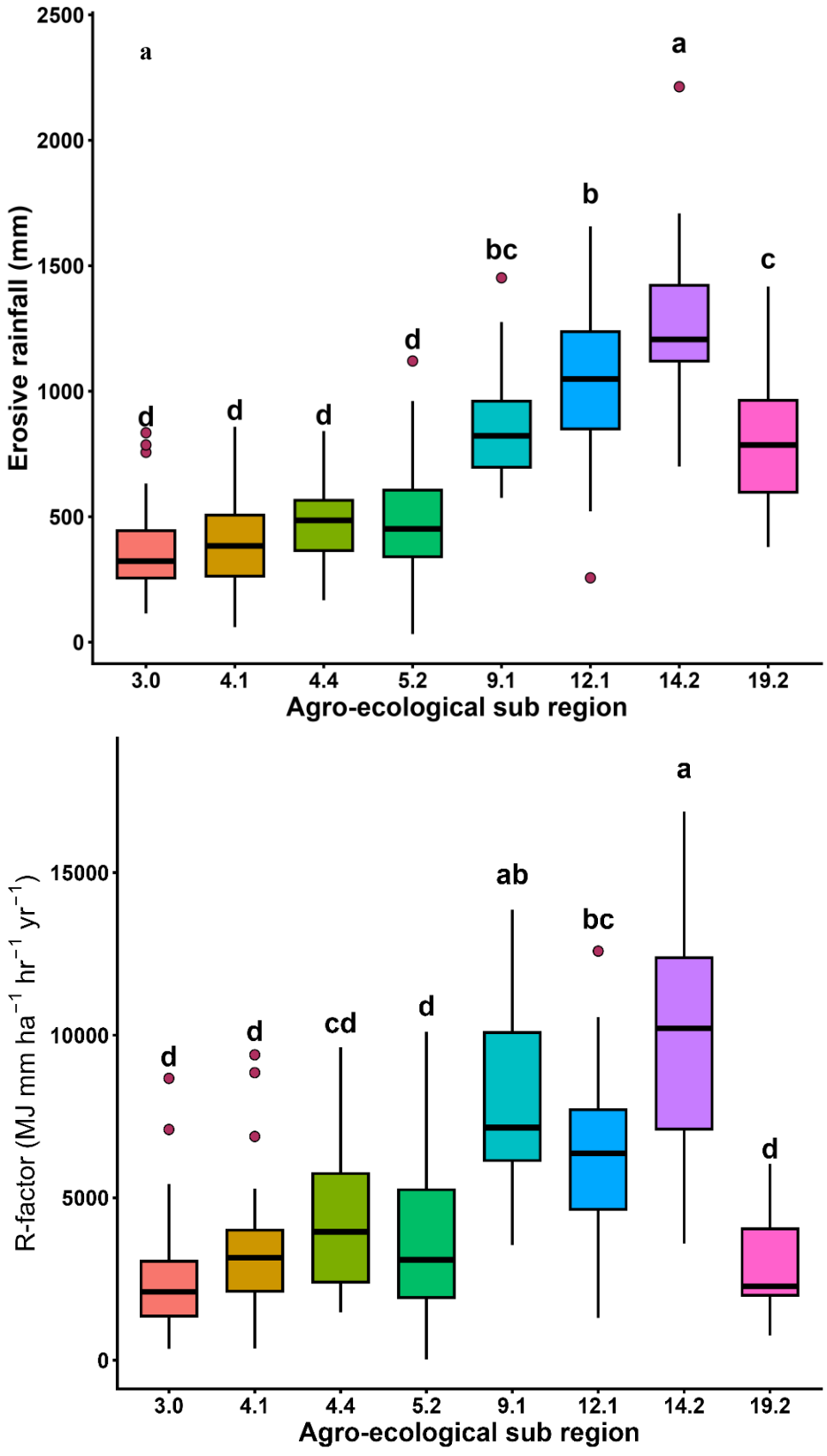

Figure 2. Box-and-Whisker plots depicting the distribution of erosive rainfall (a) and I_{30}-derived rainfall erosivity (R-factor) (b) across the selected agro-ecological sub-regions (AESRs) of India.

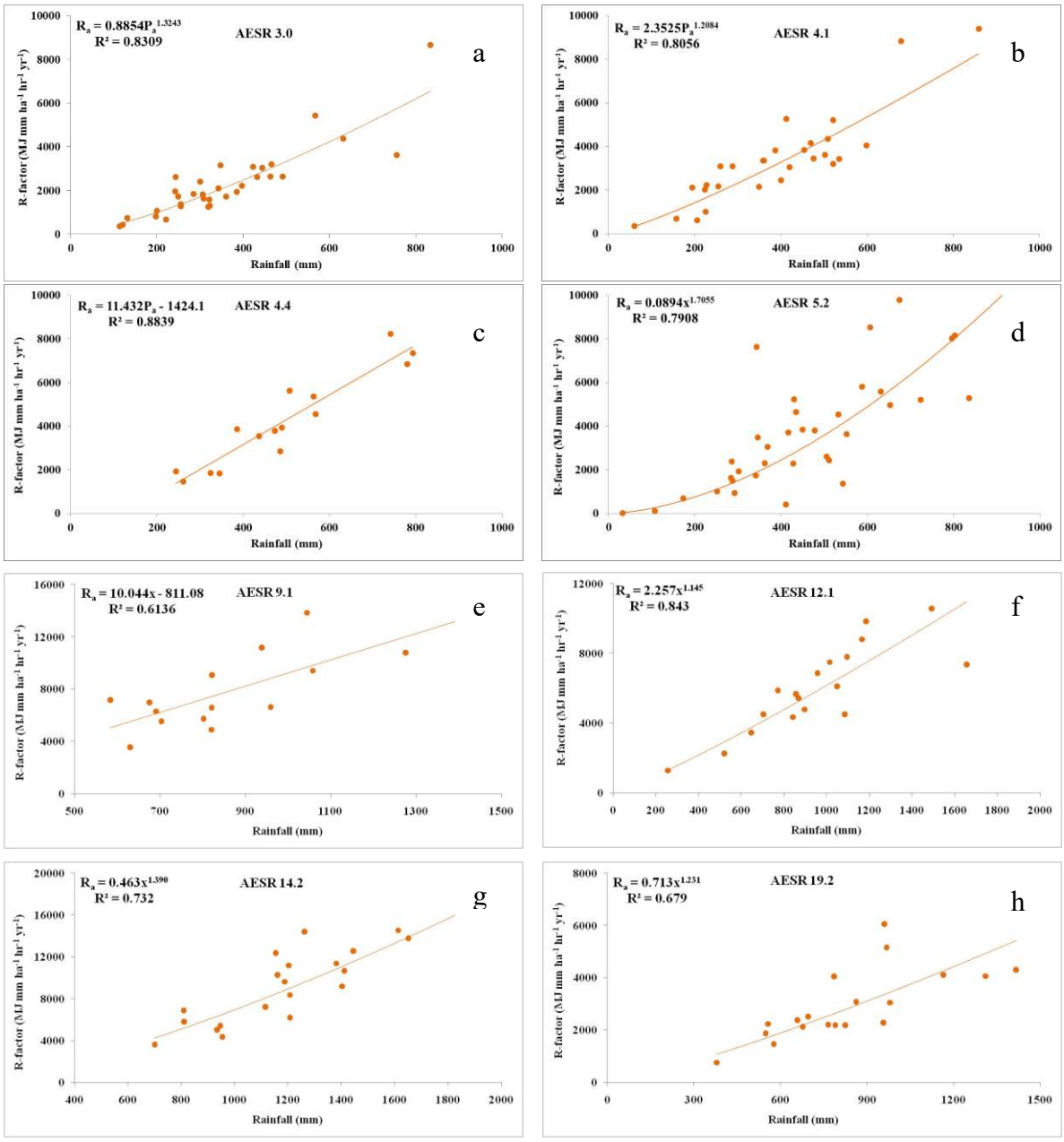

Figure 3. Best-fit empirical models illustrating the relationship between annual rainfall and rainfall erosivity (R-factor) across the selected agro-ecological sub-regions (AESRs) of India.

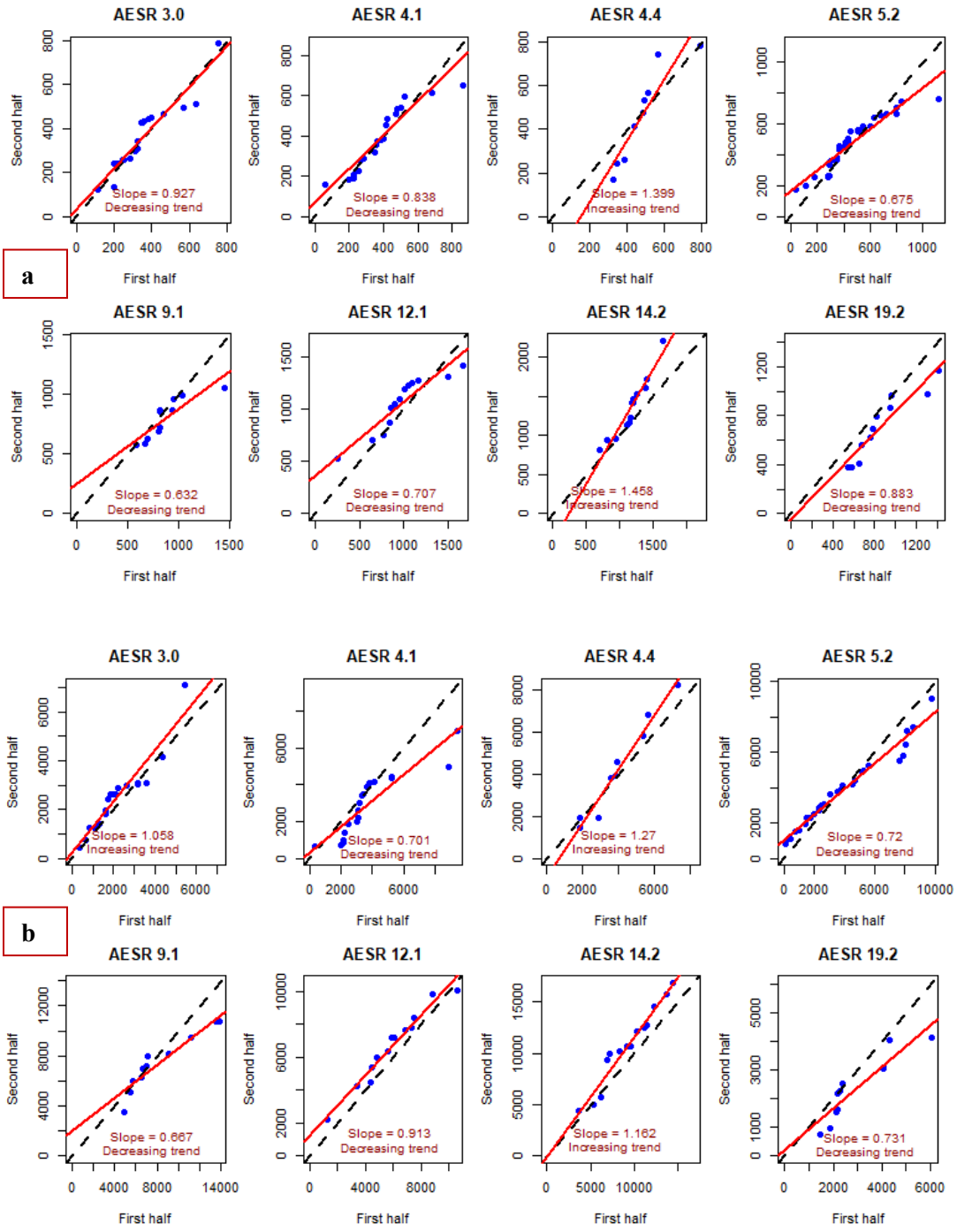

Figure 4. Innovative Trend Analysis (ITA) illustrating temporal trends in annual erosive rainfall (a) and I_{30}-derived rainfall erosivity (R-factor) (b) across the selected agro-ecological sub-regions (AESRs) of India.

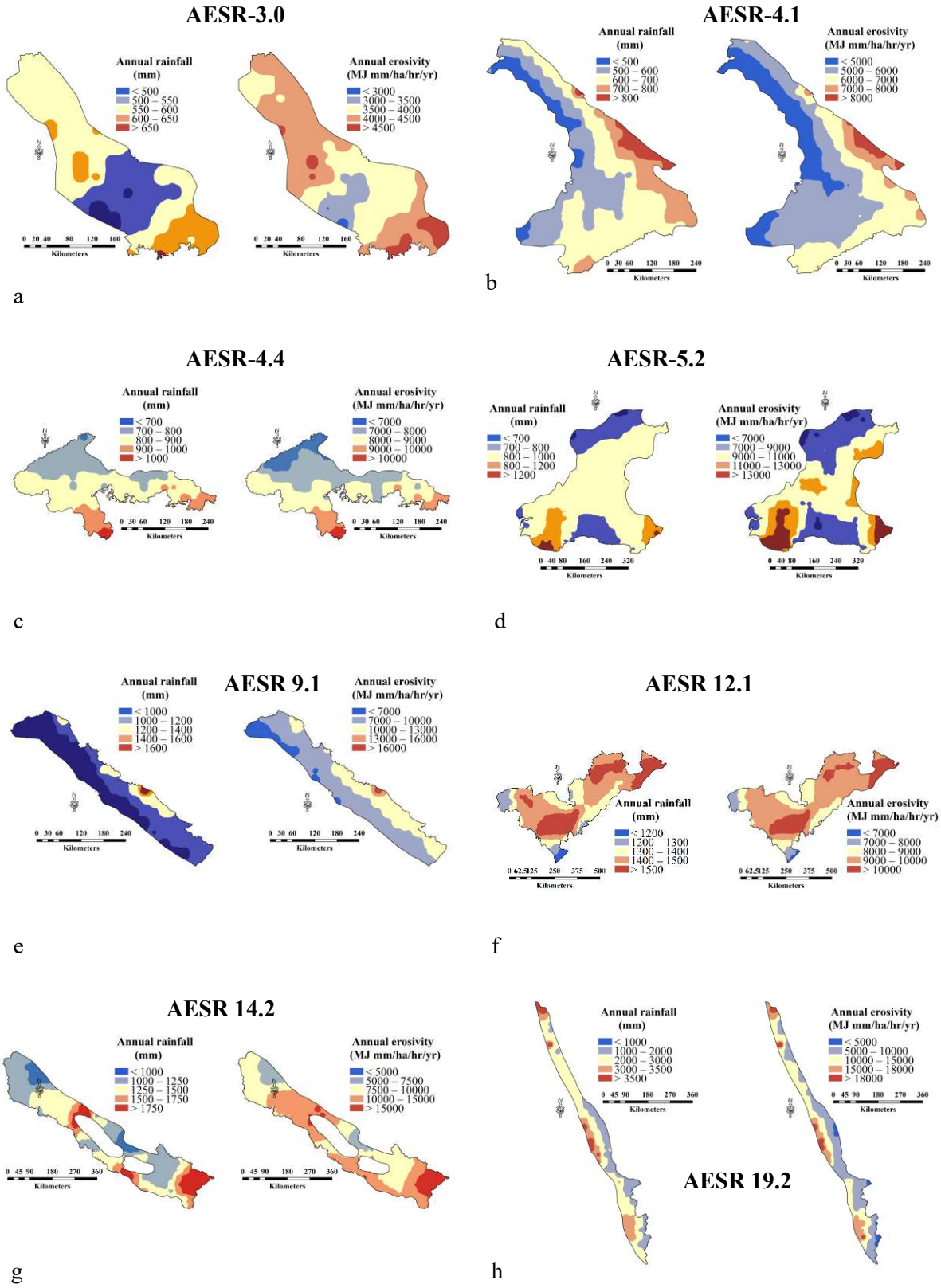

Figure 5. Spatial distribution of mean annual rainfall and model-derived rainfall erosivity (R-factor) across the selected agro-ecological sub-regions (AESRs) of India.

13

14

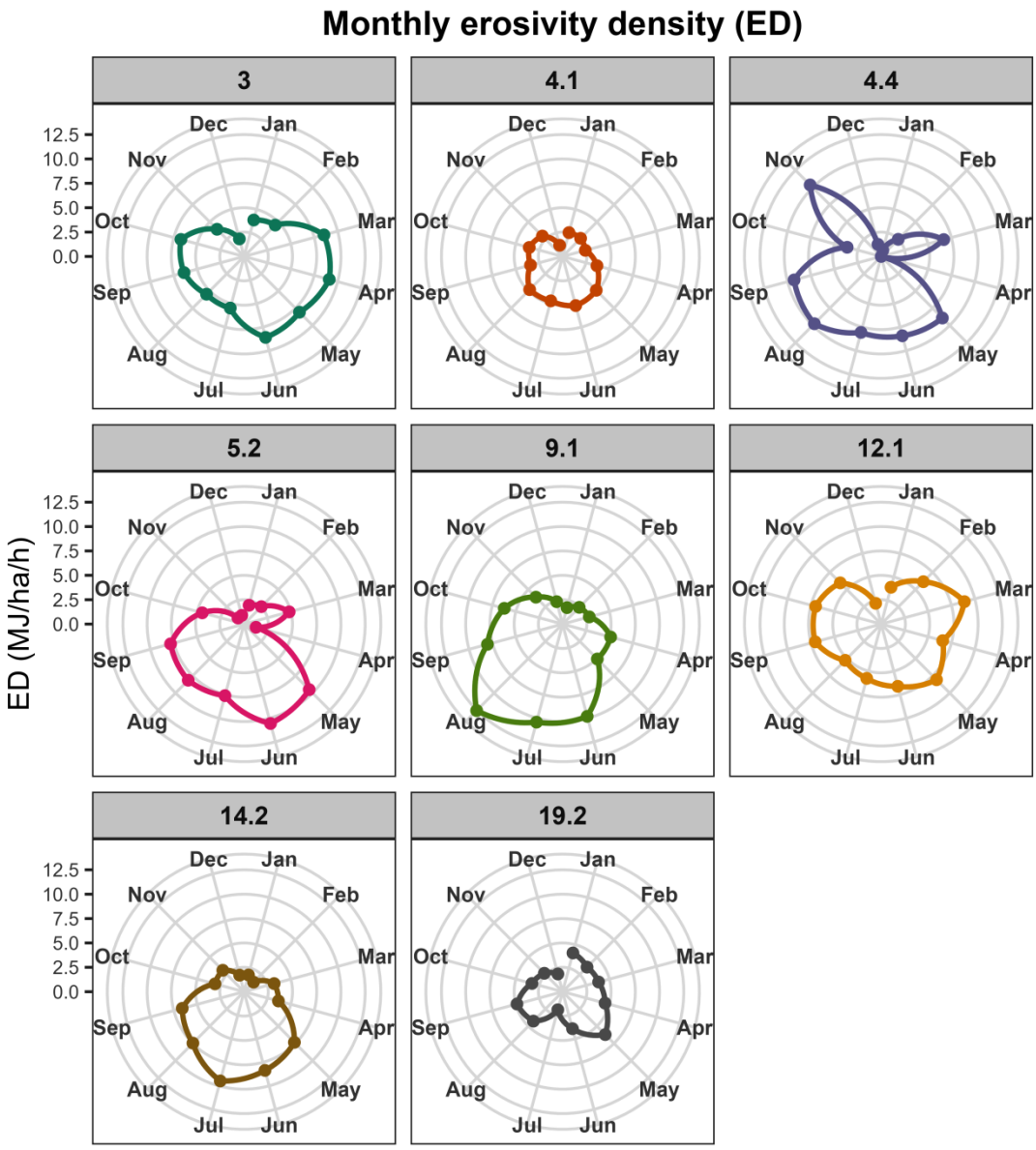

ata across the

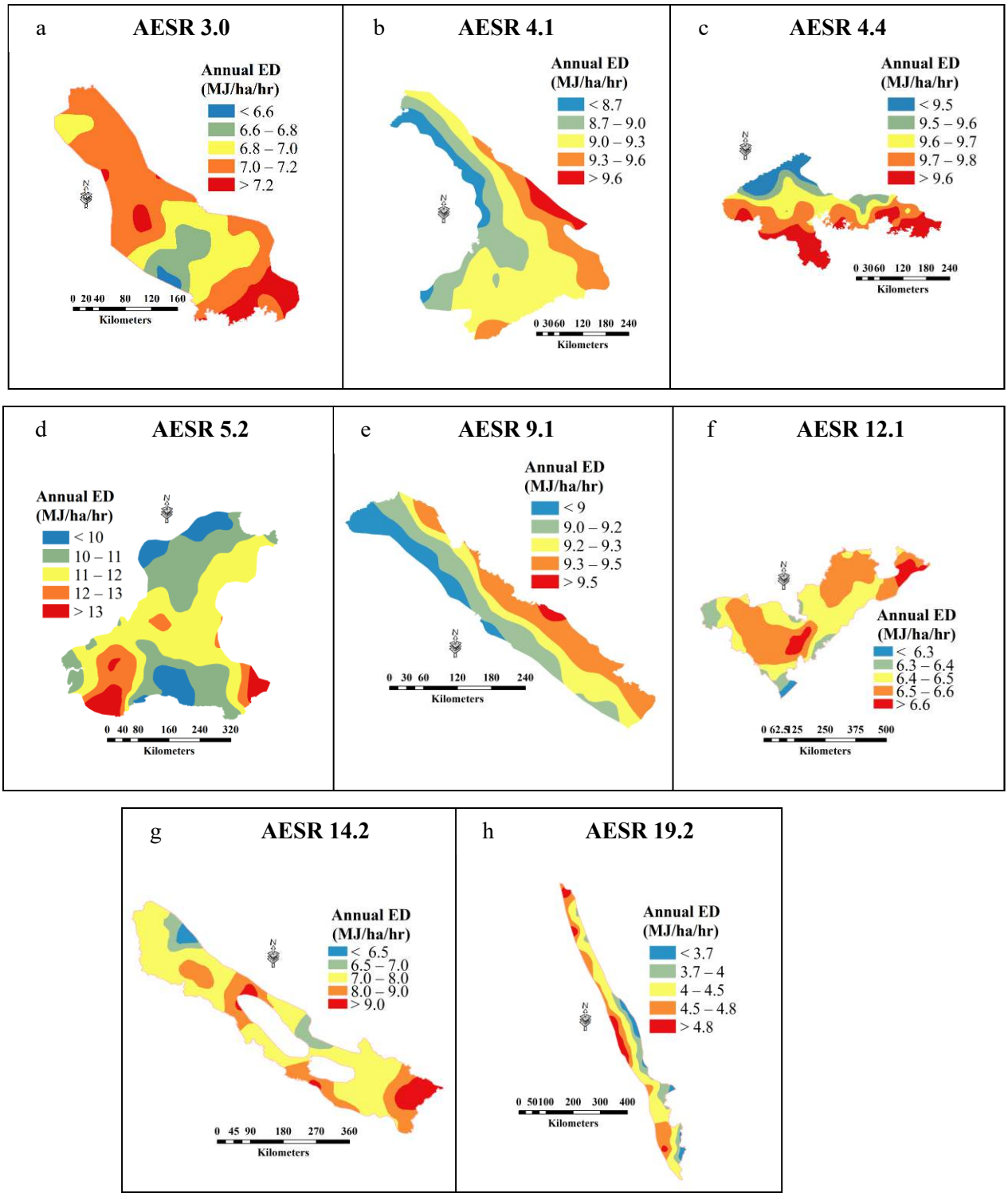

Figure 7. Spatial distribution of annual erosivity density (ED) across the selected agro-ecological sub-regions (AESRs) of India.

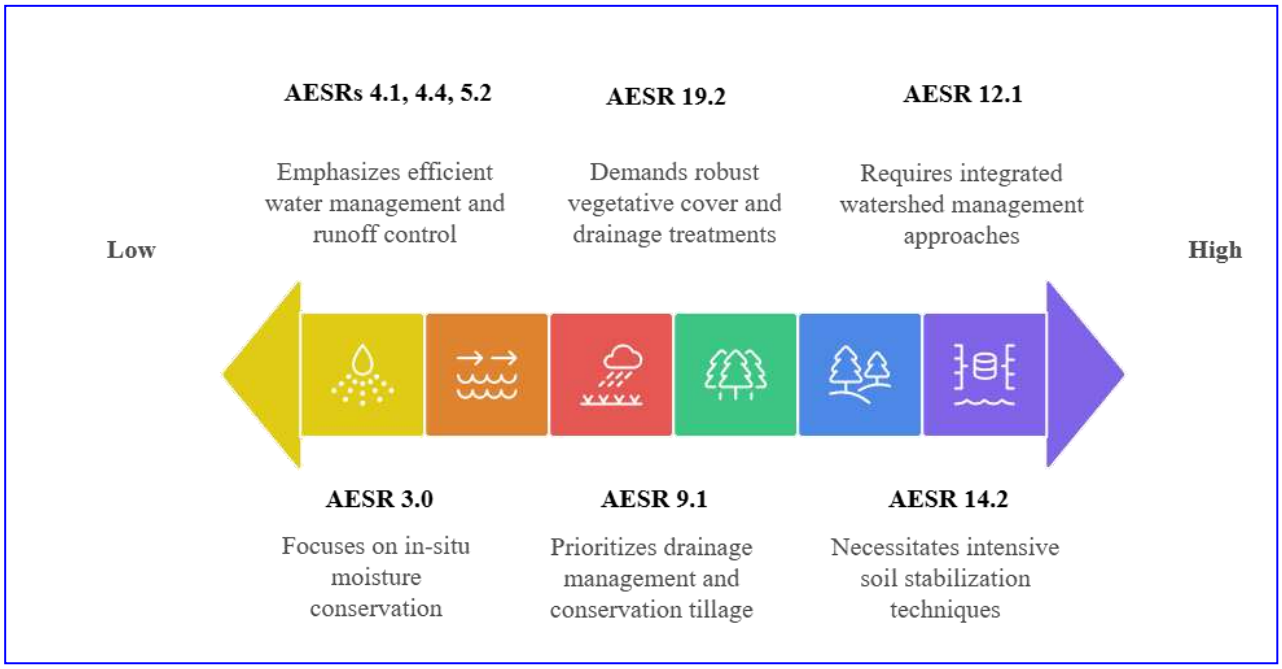

Figure 8. Suggested soil and water conservation strategies tailored to different agro-ecological sub-regions (AESRs) of India.